

# **Polarization Anisotropy, Frequency Dependent Emission, and Transport Properties of Dielectrophoretically Aligned CdSe Nanowire Arrays**

Ronghui Zhou<sup>1</sup>, Hsueh-Chia Chang<sup>1,\*</sup>

<sup>1</sup>Department of Chemical and Biomolecular Engineering, Center for Microfluidic and Medical Diagnostics

Vladimir Protasenko<sup>2</sup>, Masaru Kuno<sup>2,\*</sup>

<sup>2</sup>Department of Chemistry and Biochemistry, Notre Dame Radiation Laboratory

Amol Kumar Singh<sup>3</sup>, Debdeep Jena<sup>3</sup>

<sup>3</sup>Department of Electrical Engineering

University of Notre Dame, Notre Dame, IN. 46556

\*Corresponding authors: [hchang@nd.edu](mailto:hchang@nd.edu), [mkuno@nd.edu](mailto:mkuno@nd.edu)

Keywords: CdSe, nanowire, AC dielectrophoresis, alignment, fluorescence enhancement, ground state dipole, induced dipole, polarization anisotropy, single nanowire

## **Abstract**

Positive AC dielectrophoresis (DEP) is used to align ensembles of CdSe nanowires (NWs) near patterned micro-electrodes. Such wires, with the same crystal structure as CdSe quantum dots (QDs) and nanorods (NRs) but with significantly larger aspect ratios and sizable induced and intrinsic dipole moments, have a DEP mobility 10~100 times higher than other materials of the same dimension. As a consequence, they rapidly self-assemble in an AC electric field. The alignment also affects the fluorescence properties of the nanowires, revealing a high degree of polarization anisotropy in both the absorption and emission. An unexpected outcome of our work is the reversible, factor of

~4, field-induced, frequency-dependent enhancement of the nanowire emission. This behavior stands in contrast to the general expectation that electric fields will quench the NW emission due to the reduced spatial overlap between electron and hole wave functions. Such field-enhanced and frequency-dependent emission in aligned NWs may have potential applications in displays, as well as in optical switches and nanowire-based sensors.

### ***Introduction***

A great deal of research in nanostructures (nanocrystals, nanowires) has focused on demonstrating that these materials can be employed in devices such as field-effect transistors, photodetectors, and light-emitting diodes, in a manner akin to uses of conventional bulk solids.<sup>1</sup> At the same time, solution-based semiconductor nanostructures such as CdSe nanowires (NWs)<sup>2,3</sup> colloidal quantum dots (QDs) [or nanocrystals (NCs)]<sup>4</sup> offer added degrees of freedom, distinct from bulk behavior. In principle, these properties can be exploited and thus represent a paradigm shift for device applications. For example, nanostructures suspended in a dielectric medium can be reversibly moved in and out of solution using external stimuli<sup>5</sup>, forming conductive as well as optically active networks in precisely defined regions of a substrate.<sup>6</sup> This controllable self-assembly, coupled to size-dependent optical and electrical properties,<sup>2</sup> opens up powerful new capabilities for nanostructure-based devices.

Among low dimensional materials, semiconductor NWs exhibit strong photoconductivity<sup>7,8</sup>, as well as visible fluorescence<sup>9,10</sup>, due to their direct band gap nature. They do not suffer from problems associated with admixtures of metallic and

semiconducting species, commonly encountered in carbon nanotubes (CNTs).<sup>11</sup>

Furthermore, they can be made to emit in the visible by suitably modifying the size and shape of the nanostructure.<sup>12</sup> These dependencies have been theoretically modeled for quasi one-dimensional systems such as semiconductor nanorods (NRs).<sup>13</sup>

Because CdSe NWs have the same crystal structure as corresponding NRs and QDs, albeit with larger aspect ratios, they have similar optical properties. However, significant differences between NWs and NRs (or NCs) exist, including the presence of 1D excitons<sup>14,15</sup>, potential dielectric contrast effects<sup>14,15</sup>, enhanced 1D exciton binding energies<sup>15</sup>, variations in the effective fluorescence quantum yield, and strong changes in the density of states underlying the linear absorption. An additional difference, important but seldom noted, is the fact that NWs possess potentially significant induced and/or permanent dipole moments due to their highly anisotropic shapes. In this respect, NW aspect ratios can reach values of  $10^3$  or more due to their narrow diameters ( $< 10 \text{ nm}$ ) and micron long lengths.<sup>2,3</sup> When coupled to the presence of a polar wurtzite (W) phase, CdSe NWs, grown along the c-axis ( $<0001>$  direction) can therefore behave as giant electrets in the absence of an external electric field. More specifically, hexagonal CdSe possesses a spontaneous polarization on the order of  $P \sim 0.2\text{-}0.6 \text{ } \square\text{C/cm}^2$ . (Actual literature estimates are  $P=0.19^{16}$ ,  $P=0.42^{17}$ , and  $P=0.6^{18} \square\text{C/cm}^2$ .) These numbers are comparable to some of the largest values seen in wurtzite III-V semiconductors such as GaN ( $\sim 3 \square\text{C/cm}^2$ ).<sup>19</sup> Even in CdSe NWs with admixtures of wurtzite and zinc-blende (ZB) as well as twinned ZB sections<sup>3</sup>, many smaller dipoles might exist within individual wurtzite links (all aligned end to end along the NW length), giving rise to a significant permanent dipole.

As a consequence, both this intrinsic dipole moment as well as the strong polarizability of the wires can be exploited in tandem with classic AC dielectrophoresis to induce the alignment of NW ensembles. Such field-induced alignment, as well as assembly, may then provide a simple but effective means of manipulating and spatially controlling the NW position. This effect has previously been demonstrated in the alignment of metal NWs by dielectrophoresis.<sup>20</sup> The approach thus complements existing techniques for manipulating nanowires and/or CNTs, including Langmuir Blodgett<sup>21,22,23</sup> and microfluidic alignment.<sup>24,25</sup>

In our study, positive AC dielectrophoresis is used to align CdSe NWs. Visual confirmation of NW alignment is made through subsequent brightfield and epifluorescence measurements. We observe that aligned CdSe NWs form 3-dimentional structures instead of the more common planar structures characteristic of aligned carbon nanotubes.<sup>24</sup> These aligned assemblies exhibit strong polarization anisotropies in both the absorption and emission. Furthermore, an unexpected enhancement of the NW emission, by a factor of ~4, is observed in the presence of an electric field. This behavior is unexpected as such a field is generally expected to quench any emission due to the reduced spatial overlap between electron and hole wavefunctions<sup>26</sup>, though it is possible that enhanced 1D exciton binding energies could suppress this effect.<sup>15</sup>

From a device standpoint, ensembles of aligned NWs can be used to promote the capture of pathogens such as bacteria<sup>24</sup> both at the ensemble and single particle levels. In this respect, the enhanced field at the end of the NW can promote pathogen-NW dipole-induced “docking” as supported by our earlier work on the DEP trapping of CNTs and CNT/bacteria mixtures.<sup>24</sup> Underlying this phenomenon is an induced dipole-induced

dipole attraction with an interaction potential energy of  $\sim$ 50 kT as calculated from their dielectrophoretic velocity. Furthermore, given the direct band gap emission of the wires, changes in their emission intensity after pathogen docking may provide an alternative means of sensing apart from standard conductivity measurements.<sup>1</sup> The assembly of NW ensembles under an applied AC electric field, their fluorescence behavior both in the presence and absence of the field as well as their corresponding transport properties are therefore of practical interest for display, optical switching and sensing applications.

## **Experimental**

Narrow diameter (<10 nm) CdSe NWs with lengths between 1-10  $\mu$ m were synthesized using a seeded solution approach.<sup>2,3</sup> The asymmetric growth is catalyzed in the presence of mild coordinating surfactants such as trioctylphosphine oxide (TOPO), using low melting, bimetallic Au/Bi core/shell NPs. Such bimetallic Au/Bi catalysts have also been used in the solution phase synthesis of other NWs including PbSe and more recently CdTe.<sup>27</sup> Resulting CdSe NWs have diameters between 7-10 nm, corresponding diameter distributions on the order of 25% and intrawire diameter distributions between 3-6%.<sup>3,9</sup> Lengths exceed 10  $\mu$ m in some cases. Nanowires with branched morphologies can also be made using variations of the approach, involving different initial metal to chalcogen precursor ratios.<sup>3</sup> In all cases, NW surfaces are passivated with organic ligands such as trioctylphosphine oxide, trioctylphosphine and octanoic acid. As a consequence, the recovered NWs can be re-suspended in common organic solvents such as toluene or chloroform.

The gold micro-electrodes employed in this study were patterned using standard photolithography. Specifically, 5 nm of titanium was sputtered onto a microscope

coverslip as an adhesion layer for the subsequent evaporation of 45 nm of Au. Masks were then used to define interdigitated electrodes with a 20-40  $\mu\text{m}$  gap. A piece of cover well was glued above the electrodes to create a  $\sim$ 100  $\mu\text{L}$  perfusion chamber. This prevented samples from drying too quickly during subsequent alignment experiments. AC electric fields with magnitudes ranging from 1 to 40 kV/cm were generated using a function generator connected to a high voltage amplifier. Corresponding AC frequencies were varied between 0.2 Hz and 10 MHz.

Transport properties of aligned nanowires were studied through I-V measurements taken on an Agilent 4155B semiconductor parameter analyzer. The applied bias ranged from -40 to 40 V with obtained currents in the 100 pA range. Samples for these measurements were prepared by first aligning the wires between the interdigitated electrodes and letting the solvent dry with the field on. Some samples were also processed via rapid thermal annealing in order to improve the contact between the wires and the electrodes. All measurements were conducted under ambient conditions.

Fluorescence measurements, both during and after NW alignment, were carried out using a modified, single molecule sensitive, inverted optical microscope. The excitation source is the 488 nm line of an air cooled Ar<sup>+</sup> ion laser, filtered to remove any residual plasma light. The light is then passed through a polarization preserving single mode fiber to ensure a Gaussian TEM00 mode. It is then re-collimated with a microscope objective, effectively expanding the beam's waist to  $\sim$ 8 mm. The orientation of the light's linear polarization is controlled using a half wave plate mounted on a rotation stage. A quarter waveplate is subsequently inserted after the  $\lambda/2$  plate to create circularly polarized light for subsequent emission polarization anisotropy experiments. These experiments also

involve placing an additional linear polarizer (analyzer) prior to the detector.

The microscope can be operated confocally by overfilling the back aperture of the 1.4 NA oil immersion objective with collimated light. Alternatively, for epi-illumination, a  $f = 250$  mm lens is inserted to focus the light prior to the objective's back aperture. This creates a wider excitation area on the sample, with a field of view reaching 30  $\mu\text{m}$  in diameter. Typical excitation intensities used in our experiments range from 1 to 100  $\text{W/cm}^2$ . Emitted light from the sample is collected with the same objective and is passed through two barrier filters to remove any excess excitation light. The emission is then imaged using either a single photon counting avalanche photodiode (Perkin Elmer SPCM AQR-14) or with a Peltier cooled CCD (DVC 1412). More information about the apparatus can be found in Reference 9.

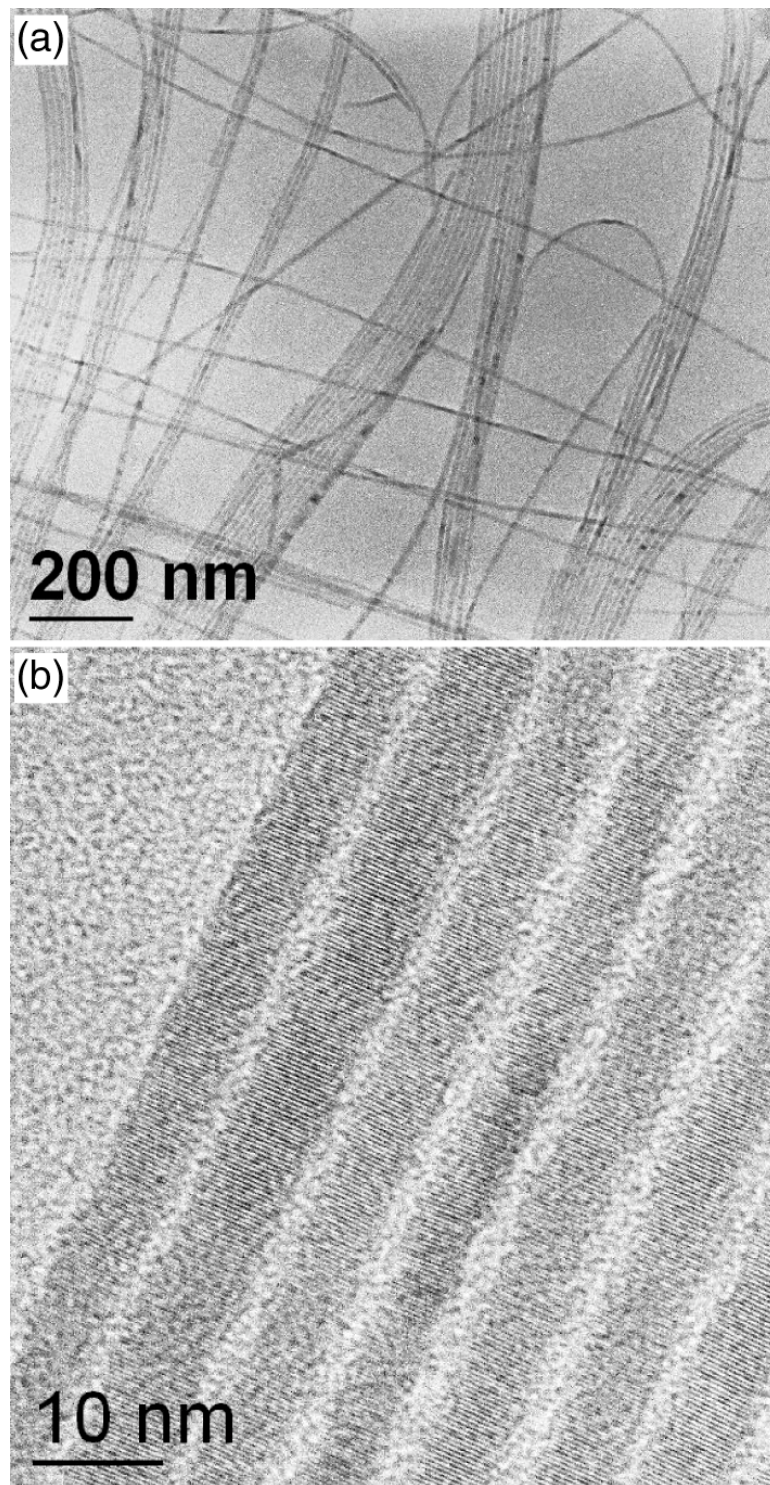


**Figure 1.** (a) Low and (b) high resolution TEM images of CdSe NWs.

### **Results and discussion**

In general, a number of ways exist for manipulating nanoscale objects using AC or DC electric fields. For example, charged particles (or nanostructures) in solution can

directly undergo electrophoresis in the presence of a uniform DC field. By contrast, nanostructures with a permanent dipole moment simply orient along the field lines due to the equal but opposing forces pulling on either side of the dipole. To manipulate neutral particles or those with permanent dipoles, AC dielectrophoresis employs large field gradients to selectively move and/or position the particles in a liquid dielectric medium.<sup>25</sup> Specifically, when a highly polarizable, but uncharged, object such as a nanowire is subjected to an electric field, an induced dipole moment is created, enabling the object to respond to electric field gradients that are present.

In the current study, the NWs of interest are shown in Figures 1 ( a,b). Figure 1a is a representative low resolution TEM micrograph of a typical ensemble where NW diameters range from 7-8 nm and lengths exceed 1  $\mu$ m. Corresponding diameter distributions are on the order of 25-30%. Figure 1b shows that the wires are crystalline and uniform, with intrawire diameter variations on the order of 3-6%.<sup>3</sup> Although the high resolution micrograph (Figure 1b) shows that the wires are crystalline, it hides the fact that individual NWs exhibit admixtures of zincblende and wurtzite phases. This can be seen in properly oriented ( $<110>$  zone) wires, as described in more detail in Reference 3.

The dielectrophoretic behavior of NWs can be treated within the context of a Maxwell-Wagner formalism. Specifically, both NWs and their surrounding medium are modeled as capacitors (dielectrics) and resistors (conductors) in parallel. Differences in conductivity and dielectric constant of the NW relative to its surrounding medium enable the creation of induced charges at either end of the wire in the presence of an electric field. The magnitude of this induced dipole can be calculated using

$$\square_{ind}(t) = \square_0 \square_m V_{NW} KE(t) \quad (1)$$

where  $\square_m$  is the dielectric constant of the medium,  $\square_0$  is the vacuum permittivity, and  $V_{NW}$  is the NW volume.  $K$  is the complex Clausius-Mossotti factor, which depends on the complex dielectric constant of the NW and that of the surrounding medium. Simplifying the above expression is the significantly larger longitudinal polarizability of a NW relative to its transverse (radial) polarizability. As a consequence,  $K$  for a nanowire with a corresponding Lorentz depolarization factor of  $n \sim 0^{29}$  can be approximated by

$$K = \frac{(\square_{NW}^* \square \square_m^*)}{\square_m^*}. \quad (2)$$

The complex dielectric constant  $\square_{NW(m)}^* = \square_{NW(m)} \square i \square_{NW(m)} / \square$  of both the NW and its surrounding medium is expressed in terms of their respective conductivities,  $\square_{NW(m)}$ , as well as the angular frequency of the applied field,  $\omega$ . As a simple approximation to the magnitude of the induced dipole, we consider a 10 nm diameter, 1 μm long NW dispersed in chloroform and use the relevant parameters  $\square_{NW}=10.2^{16}$ ,  $\square_m=4.8$  and  $E = 5 \times 10^3 V/cm$ . From this and Equations 1 and 2 one finds that  $\square_{ind} \sim 560 D$ , suggesting that the NWs can indeed be manipulated using an external field.

The dielectrophoretic force on the wire, due to the interaction between its dipole moment and the electric field gradient, can be expressed by<sup>29</sup>

$$F_{DEP} = \square(t) \cdot \square E(t) = \frac{1}{2} (\square r^2 L) \square_m \operatorname{Re}\{K\} \square |E_{rms}|^2 \quad (3)$$

where  $E_{rms}$  is the root mean square value of the electric field and the cylinder volume is calculated using its radius,  $r$ , and length,  $L$ . The direction of DEP motion depends on the

sign of the Clausius-Mossotti factor  $K$ . This parameter captures the field-induced polarization due to both internal and external contributions as well as that due to the capacitive charging current of the double layer.<sup>30</sup> Depending on the orientation of the dipole relative to the AC electric field as well as the permittivity and conductivity of the NW/medium, the wire can move towards either the high (positive DEP) or low (negative DEP) field region.

Equations (4) and (5) show both the high and low frequency limits of the real part of  $K$ .

$$\text{Re}\{K\} = \frac{(\underline{\epsilon}_{NW} - \underline{\epsilon}_m)}{\underline{\epsilon}_m} \quad (\underline{\epsilon} \gg 1) \quad (4)$$

$$\text{Re}\{K\} = \frac{(\underline{\epsilon}_{NW} - \underline{\epsilon}_m)}{\underline{\epsilon}_m} \quad (\underline{\epsilon} \ll 1) \quad (5)$$

and explain why CdSe NWs in chloroform maintain a positive DEP force at all frequencies investigated. Namely, CdSe has substantial dielectric constants,  $\underline{\epsilon}_{NW}=10.2$  ( $\underline{\epsilon}=9.33$ , transverse direction)<sup>16,31</sup>, and conductivities ( $\sigma_{NW}=16.7 \mu\text{S}/\text{cm}$ )<sup>7</sup> relative to its surrounding medium. By contrast, chloroform has a relative dielectric constant of  $\underline{\epsilon}_n=4.8$  and a corresponding conductivity of  $\sigma_m=0.02 \mu\text{S}/\text{cm}$ . As a consequence,  $K$  is positive for all frequencies considered and accounts for why CdSe wires always move towards, not away from, the electrodes. From this we can also estimate the effective NW DEP velocity to be on the order of 10  $\mu\text{m}/\text{s}$ , taking into account viscous drag due to the solvent (chloroform viscosity  $\eta \sim 0.38$  centistokes). Although this value is in line with an experimentally derived DEP (lower limit) velocity of  $\sim 8.8 \mu\text{m}/\text{s}$ , many wires have velocities much faster than this, suggesting additional contributions to the NW mobility.

In this respect, the true DEP velocity can be much higher than that calculated above due to the presence of a permanent dipole in CdSe NWs. More specifically, we estimate that a 10 nm diameter wurtzite CdSe NW possesses an intrinsic dipole moment of roughly  $50*L$  Debye, where  $L$  the length of the nanowire expressed in nm. Based on conservative estimates of the spontaneous polarization for CdSe,  $P \sim 0.2 \text{ } \mu\text{C/cm}^2$ , a 10 nm diameter wire has a total surface charge density of  $\sigma = 1.25 \times 10^{12} \text{ e/cm}^2$ . The product of this and the surface area normal to the wire growth axis gives  $\sim 1$  electron per NW face. The corresponding dipole moment is then  $D = (1.602 \times 10^{19} \text{ C})(1 \times 10^{19} \text{ m/nm})(L)/3.336 \times 10^{30} \text{ C} \cdot \text{m}/\text{D}$  or  $48*L$  Debye for a pristine 10 nm diameter wurtzite CdSe NW, grown along the <0001> direction in vacuum. Recent experimental results corroborate this result, suggesting the presence of a permanent dipole moment in CdSe QDs and NRs with comparable magnitudes. For example, Guyot-Sionnest has found ground state dipoles ranging from 20-50 D<sup>18</sup> as well as 40-100 D<sup>32</sup> in CdSe QDs. Likewise Krauss<sup>33</sup> has estimated that the magnitude of the dipole, if present in NRs, is < 350 D, comparable to the numbers found by Alivisatos (96-210 D).<sup>16</sup>

Such permanent dipoles in our NWs may then be expected to produce a net DEP velocity in excess of 100  $\mu\text{m/s}$ , which would then be consistent with the frequent occurrence of DEP velocities faster than 10  $\mu\text{m/s}$  in our experiments. However, questions still remain regarding the actual presence of a ground state dipole in CdSe nanostructures because of seemingly contradictory theoretical and experimental results that exist in the literature. In this respect, one competing explanation for the appearance of an apparent permanent dipole in CdSe stems from the presence of surface localized

charges, as described by Shim and Guyot-Sionnest.<sup>32</sup>

Along these lines, an alternative explanation for the unexpectedly large NW DEP velocities exists. Namely, the presence of mobile carriers either on or within the NW will establish a charge density at either end of the nanowire during each half cycle of the AC field. The magnitude of this charge density can exceed that induced by the external electric field as well as that due to the spontaneous polarization of wurtzite CdSe. Some evidence for these mobile carriers exist in recent NW FET experiments we have conducted, showing unintentional doping of the wires.<sup>7</sup> Furthermore, it is possible that surface localized carriers exist on the wires, given that analogous colloidal CdSe QDs have been observed to possess both positive and negative surface charges.<sup>5,32</sup> In all cases, the resulting dipole moment from these mobile charges can easily be much larger than the induced dipole moment obtained from the above Maxwell-Wagner theory. Furthermore, it can be larger than any permanent dipole moment within the wire. To illustrate, each charge localized at the end of the wire causes a 50,000 D dipole moment in a 1  $\mu\text{m}$  long NW. Such a scenario could then begin to explain the origin of the discrepancy between the predicted Maxwell-Wagner DEP velocity and that observed experimentally.

Irrespective of the actual model utilized, the large induced as well as permanent dipole moments in CdSe NWs combine to induce dipolar alignments in the presence of AC electric fields. In our experiments, an AC electric field (0.5-12 kV/cm, frequencies between 0.2 Hz and 10 MHz) was applied to NWs dispersed in chloroform. NW alignment was detected visually through both brightfield and epifluorescence measurements. Figure 2a shows a brightfield image of aligned NWs spanning a  $\sim$ 20  $\mu\text{m}$  junction. The aligned NWs clearly follow the electric field lines. Similarly, Figure 2b

shows epifluorescence images of the alignment at different stages. NW growth occurs at both electrodes as expected for a particle experiencing a positive DEP force. Movies illustrating the alignment are provided in the supporting information.

A positive DEP force is also observed at 10 MHz unlike common bioparticles, which transition from negative to positive DEP forces as AC frequencies increase towards 1~10 MHz.<sup>29</sup> The latter effect is a problem for DEP-based sensors since the low turnover frequency makes the DEP trapping field short ranged and not effective for interacting with species of interest dispersed in the medium. By contrast, the 10 MHz positive DEP force seen in NWs enables the field to spread further into the surrounding dielectric medium.

In aligned NW ensembles, we observe long-chain linear NW bundles due to dipole-dipole (end-to-end) interactions. This is similar to structures seen in single wall nanotubes (SWNTs) assembled from organic solutions.<sup>34,35</sup> Furthermore, based on simple dipole-dipole interaction considerations,  $U(r) = \frac{\mu_1\mu_2}{2\epsilon\epsilon_m r^3}$ , we obtain an estimated interaction potential energy between two side-to-side oriented 50 D wurtzite NW sections of ~0.5 eV (~20 kT). This assumes an interwire spacing of 1.1 nm based on the presence of TOPO ligands on the NW surfaces.<sup>36</sup> Such large interaction potential energies would, in turn, suggest dipole-dipole interactions as the root cause of “bundling” commonly seen in NW ensembles.<sup>2,3</sup>

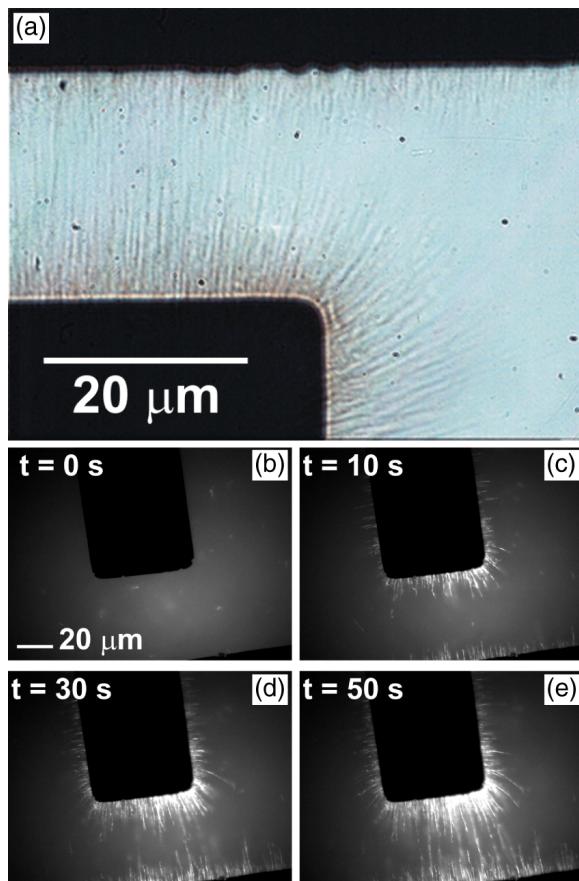


**Figure 2.** Dielectrophoretically aligned CdSe NWs using an AC electric field (10V, 1MHz) with electrodes separated by a 20  $\mu\text{m}$  gap. (a) Resulting brightfield image after alignment and (b) epifluorescence images taken at different times during the alignment.

In Figures 3 (a-c), epifluorescence images of different layers of aligned nanowire bundles are shown as one progressively moves away from the substrate and into the bulk solution. The alignment of the ensemble appears to follow the three dimensional electric field lines, causing NW bundles to arch into solution.

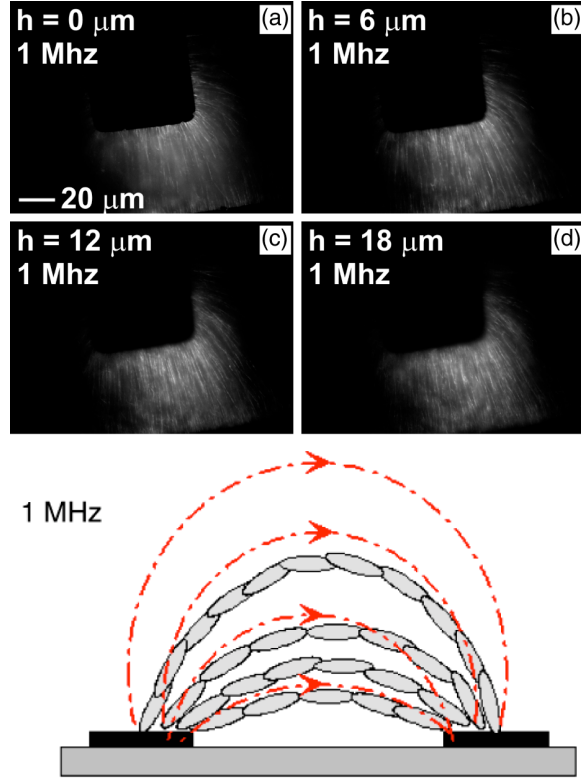


**Figure 3.** (a-d) Three-dimentional CdSe NW assemblies aligned using different AC frequencies. Images are taken at different depths into the solution, away from the substrate/solution interface. The accompanying cartoon illustrates the overall effect of the alignment AC frequency.

For example, near the substrate all of the NWs are more or less in the same image plane (Figure 3a). However, as one moves into the solution (Figures 3b-d), the wires become arched, seen by sections of the same wires simultaneously in and out of focus. This phenomenon is apparent since the depth of focus of the 1.4 NA objective is on the order of 180 nm. The arched structure persists into the bulk solution until it fades out above the electrodes. A cartoon illustrating this accompanies Figure 3.

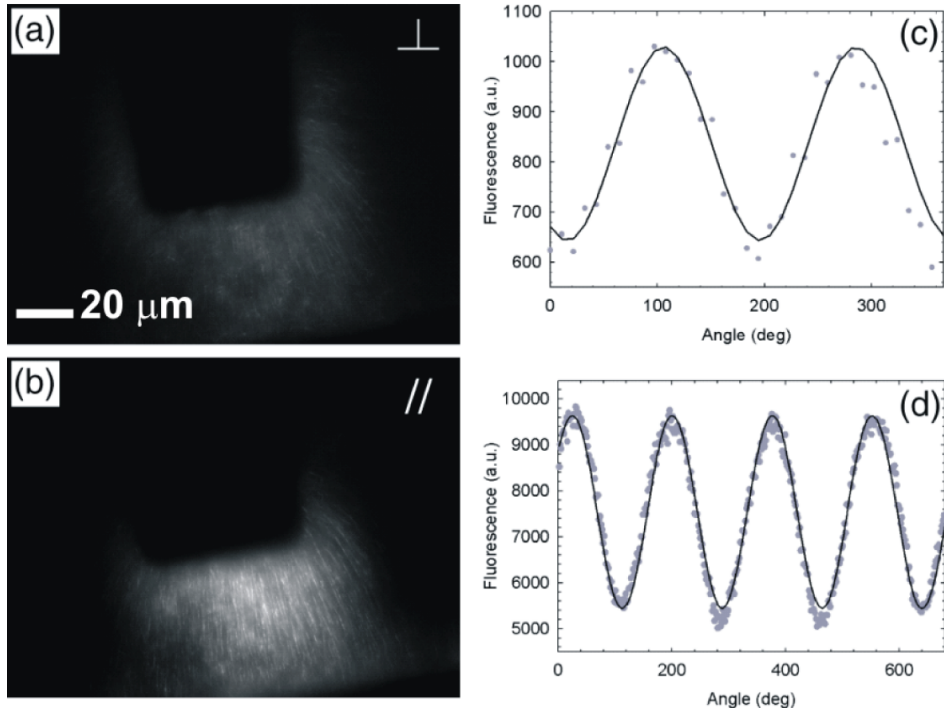


**Figure 4.** (a) Fluorescence images from the absorption polarization anisotropy of aligned NW ensembles. (b) Corresponding plot of the absorption polarization anisotropy. (c) Plot of the emission polarization anisotropy from a different aligned ensemble.

Additional characterization of aligned NW ensembles was conducted through absorption and emission polarization anisotropy measurements. In these experiments, a 1 kHz AC electric field ( $E = 5 \times 10^3$  V/cm) was first used to align the NWs, fixing their orientation. Figure 4 illustrates an example of NWs oriented between two electrodes. The linear polarization of the excitation was subsequently rotated using a  $\pi/2$  waveplate. Epifluorescence images of the ensemble (Figure 4 a,b) clearly show changes in the emission intensity with polarization angle. A movie illustrating this is also provided in the supporting information section.

Typical absorption (emission) polarization anisotropies,  $\Pi = \frac{I_{\parallel} - I_{\perp}}{I_{\parallel} + I_{\perp}}$ , of aligned samples [ $I_{\parallel(\perp)}$ ] are the intensities of the emitted light parallel (perpendicular) to the NW

length] were determined to be  $\Delta=0.24$  ( $0.27$ ) by fitting the angle dependent intensity ratio (Figure 4 c,d) to a  $\cos^2 \Delta$  function. Values for the ensemble intensity were obtained by averaging intensities from 7 random locations within the electrode gap. Although the results show significant net absorption/emission anisotropies, their values are suppressed relative to that seen in individual bundles as well as in individual NWs. To illustrate, rather than randomly sample the intensity in the electrode gap, if we focus only on the emission intensity from resolved bundles in the array, values of the absorption (emission) polarization anisotropy jump to  $\Delta=0.74$  ( $\Delta=0.60$ ). This confirms our visual observation that the actual NW dielectrophoretic alignment is incomplete despite the high degree of overall alignment (Figures 2 and 3). Furthermore, these values are consistent with both the absorption and emission polarization anisotropy of single branched CdSe NWs seen in Figure 5. Typical absorption (emission) polarization anisotropies from such individual NWs are found to be  $\Delta=0.77$  ( $\Delta=0.76$ ).

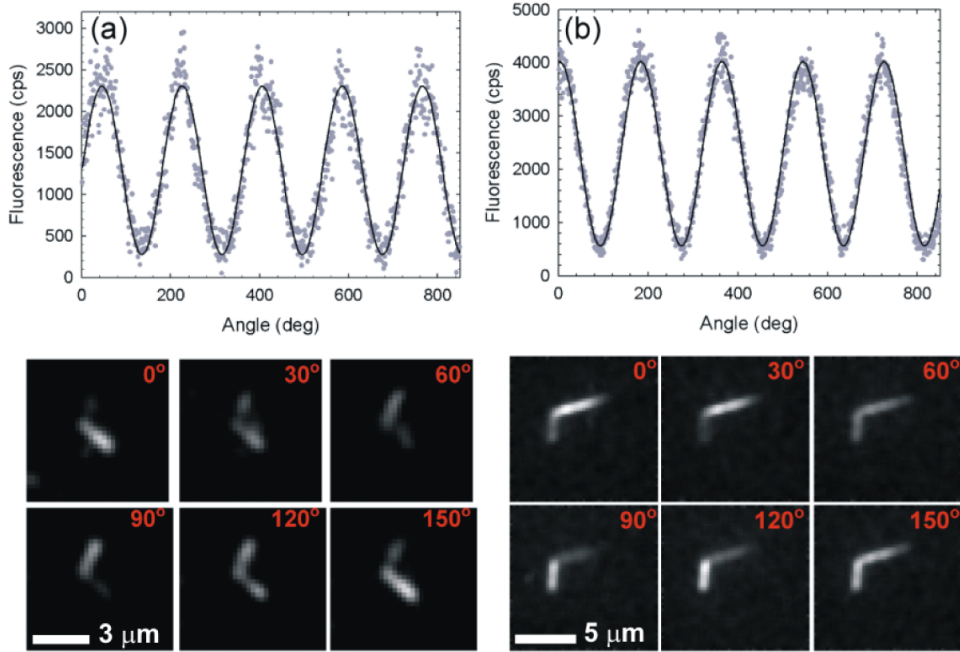


**Figure 5.** Absorption (a) and emission (b) polarization anisotropy measurements of single v-shaped CdSe NWs. Corresponding images of the NWs, at selected angles, are shown below.

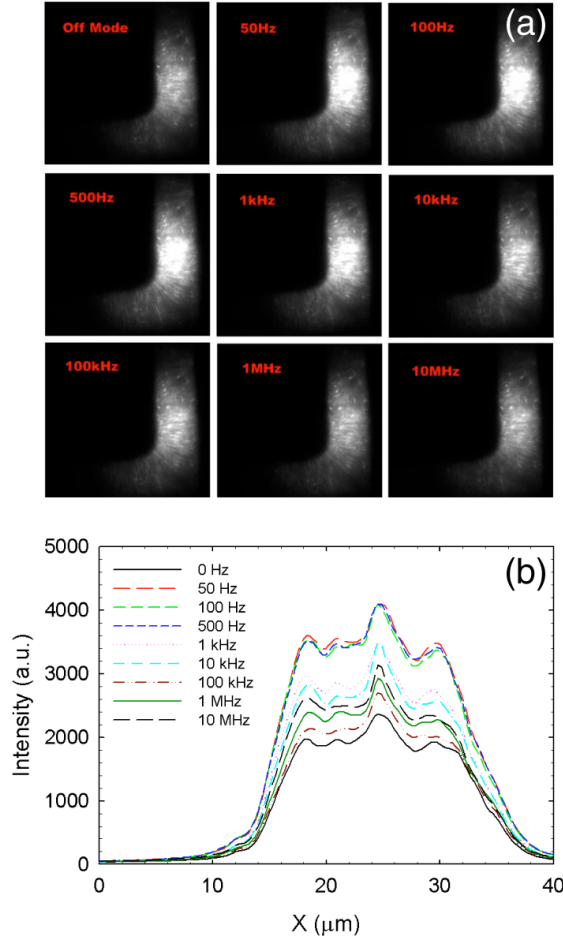


**Figure 6.** (a) Frequency dependent fluorescence images of aligned CdSe NWs between 20  $\mu\text{m}$  spaced electrodes. (b) Corresponding intensity cross section across the channel as a function of frequency.

During our measurements an unusual observation was made. Namely, we observed that the electric field caused an apparent enhancement of the NW emission. More specifically, the emission intensity of aligned NWs, measured over a range of frequencies between 0.2 Hz and 10 MHz with an AC square wave (0.5-12 kV/cm), enhances the emission by a factor of  $\sim 4$  relative to the zero field case. Figures 6 (a,b) show both images and an intensity cross section of aligned NWs as a function of frequency. The

applied electric field is 5 kV/cm. Visual growth in the emission intensity is apparent following initial increases in applied AC frequency. Higher frequencies, however, cause decreases in the enhancement, which converge to the zero field value.

This trend is shown more quantitatively in Figure 7a, which further illustrates that the same behavior is present under different electric field strengths (0.5-5 kV/cm). In all cases, a characteristic roll off frequency of  $\sim$ 10 Hz is apparent, suggesting a characteristic system response time of  $\sim$ 100 ms. Additional characterization of the phenomenon was conducted by monitoring the emission intensity while increasing the electric field strength at a given frequency. This likewise causes fluorescence enhancements up to a factor of 4. More specifically, Figure 7b shows growth of the emission intensity at four fixed frequencies when field strengths are increased to 12 kV/cm. Apparent from the figure is the fact that lower AC frequencies cause the largest fluorescence enhancements in contrast to higher frequencies, which suppress the effect.

The low frequency behavior of the emission is unexpected as previous work on single NRs under DC electric fields have shown that externally applied fields generally act to reduce the electron/hole wave function overlap, causing a decrease of the overall emission intensity.<sup>26</sup> We speculate that this enhancement effect may be related to the presence of mobile carriers on or within the NW, based on NW FET measurements<sup>7</sup> as well as observed discrepancies between predicted Maxwell-Wagner DEP velocities and those observed experimentally. Despite of our incomplete understanding of the phenomenon, the unexpected ability to enhance the emission at low frequencies and high fields offers a potentially attractive switching mechanism for both sensing and display applications.

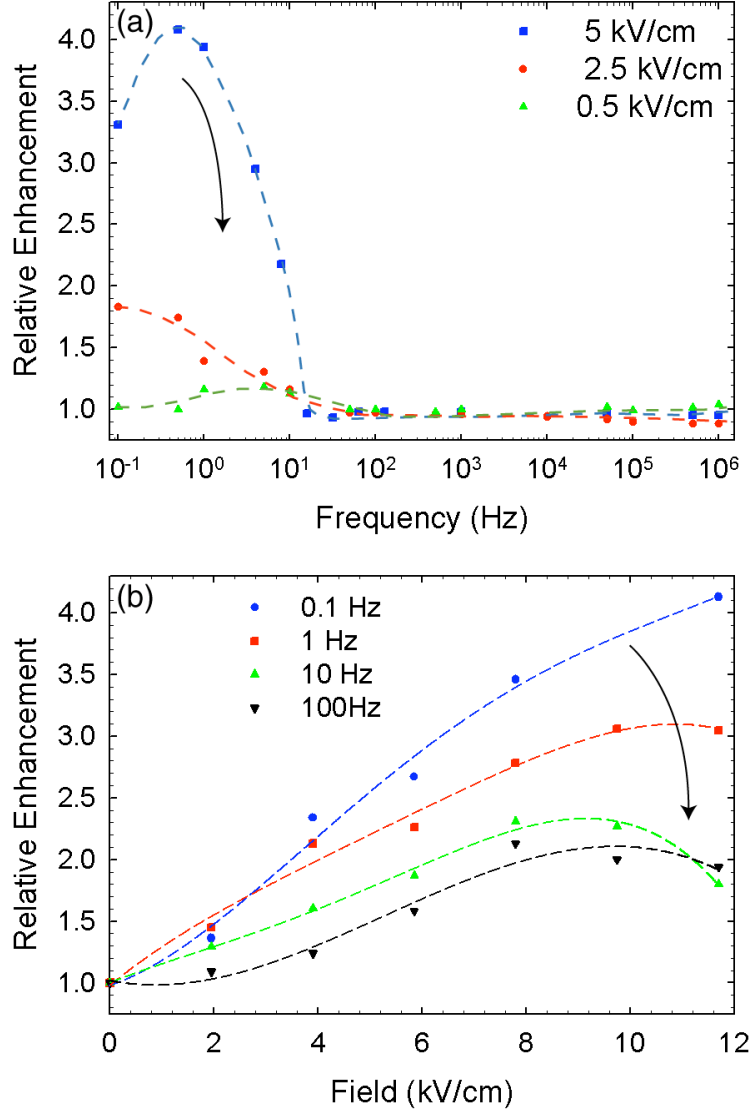


**Figure 7.** (a) Enhancements of NW emission as a function of frequency at various electric field strengths.

(b) Enhancements of the NW emission as a function of electric field strength at various fixed frequencies.

Dashed lines are guides to the eye.

In all cases, no variations of the emission spectra were observed with applied electric field. This is shown in Figure 8 where both the field dependent emission spectra of an aligned ensemble and a single wire are shown together.

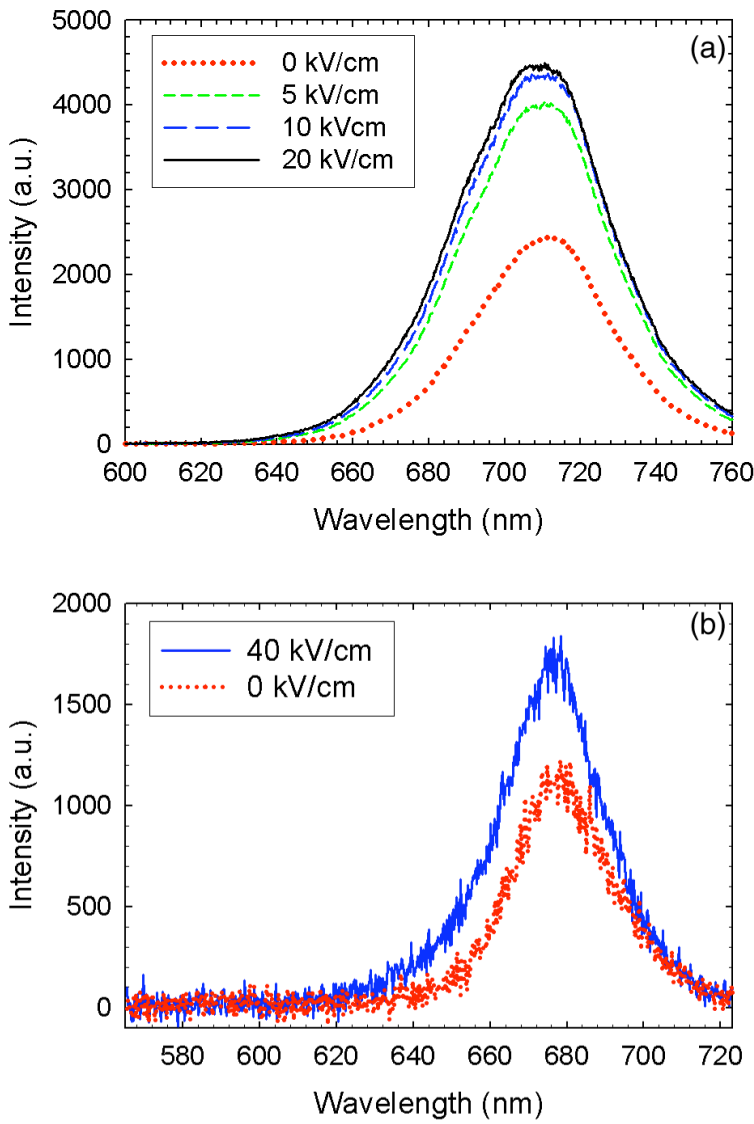


**Figure 8.** Emission spectra of (a) an aligned NW ensemble and (b) a single NW both at different electric field strengths.

While a Stark-induced redshift of the emission might be expected, it is likely absent here because of the relatively low field strengths used in these experiments (0-40 kV/cm). In this respect, previous studies measuring the quantum confined Stark effect in semiconductor QDs have employed fields exceeding 100 kV/cm to reveal spectral shifts on the order of 10 meV.<sup>37</sup> Given the low fields used in our experiments, the broad emission linewidths of both ensembles and single NWs<sup>9</sup> may conceal such small Stark

induced spectral shifts, leading to no apparent change of the spectrum with electric field.

Since aligned CdSe NW ensembles have potential real world uses, the transport properties of aligned nanowires were measured using an Agilent 4155B semiconductor parameter analyzer. Prior to any thermal treatment, the as-aligned CdSe nanowires on gold contact pads exhibited non-ohmic behavior. Currents without (with) white light illumination were <10 pA (120 pA) under an average illumination intensity of ~540 mW/cm<sup>2</sup> over the spectral range between 200 nm and 800 nm with the larger current in the presence of light indicating the strong photoconductivity of the wires.<sup>8</sup> A 40 V source-drain bias was used in both cases. The low currents and non-ohmic behavior seen in Figure 9a (bottom) under optical illumination suggests poor contact between the wires and the gold electrode. This could arise from a number of reasons including the presence of surfactant on the NW surface, which acts as an insulator.

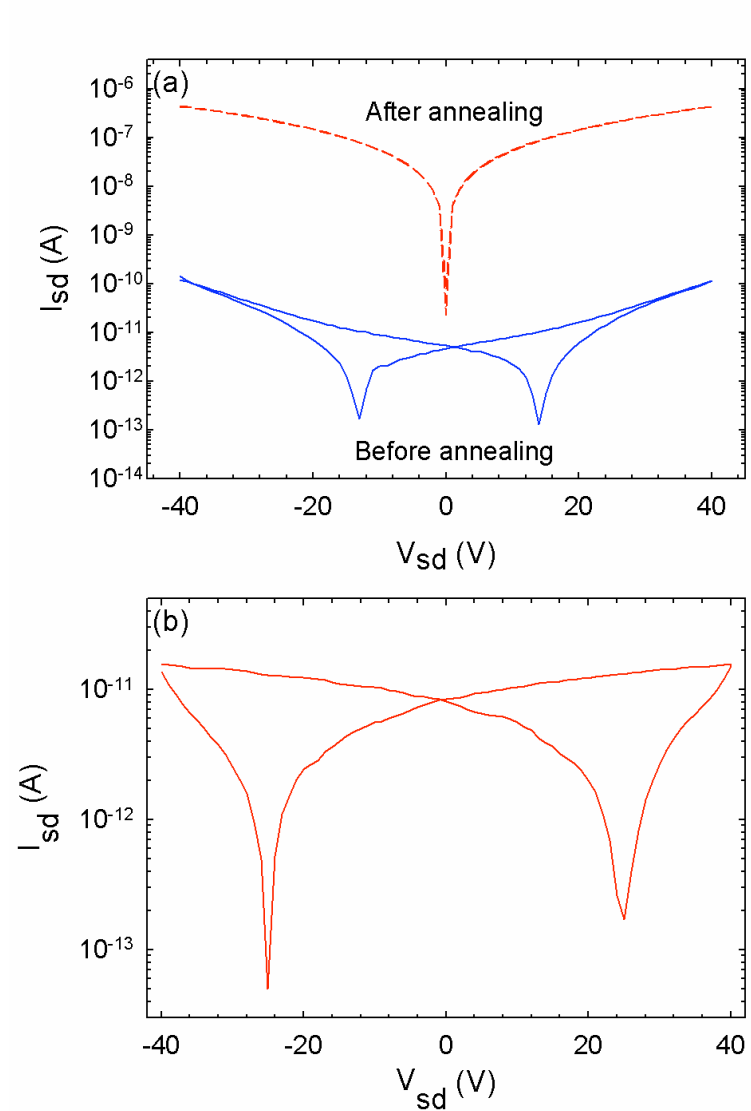


**Figure 9.** (a) Current-voltage characteristics of aligned CdSe NWs under optical illumination, both before and after rapid thermal annealing. In the latter case, a marked improvement in photocurrent is observed. (b) I-V characteristics of same device after annealing but without illumination.

After rapid thermal annealing [1 minute at 300 °C in a forming gas environment (95% N<sub>2</sub>, 5% H<sub>2</sub>)], however, the transport properties of the aligned wires improved markedly (Figure 9a, top). Ohmic behavior was observed under optical illumination and currents approached 430 nA, a three orders of magnitude improvement from the previous unannealed case. Even without illumination, currents of the annealed device approached 15 pA (Figure 9b). We attribute these improvements to three factors: (a) removal of NW

surface passivating surfactants that inhibit carrier flow between the nanowire and metal pads, (b) removal of surfactant between adjacent NWs in the aligned assembly and (c) interdiffusion of Au into CdSe forming an alloyed ohmic contact, though this remains to be verified. All suggest that such aligned CdSe NW arrays may have potential device applications.

### ***Conclusion***

We have shown that high aspect ratio CdSe NWs can be manipulated using micro-fabricated electrodes due to their large DEP mobility under an AC field. Both the large induced and permanent dipoles of the NWs promote their self-assembly into ordered assemblies whose structure is frequency dependent. Absorption and emission polarization anisotropy experiments show that the NW arrays exhibit a high degree of alignment. An unexpected observation is the sensitivity of the emission to applied electric fields. Specifically a factor of ~4 enhancement in the emission intensity is observed at low frequencies and high fields, suggesting potential uses of aligned NWs in optical switching, display technologies as well as in sensing applications. In this respect, earlier studies have shown that single viruses can be detected through NW conductivity measurements.<sup>38</sup> By the same token, the sensitivity of the NW fluorescence to environment and electric fields would suggest an additional means of detecting and perhaps even identifying captured pathogens, enabling future improvements in nanowire-based biosensors.

### ***Acknowledgements***

R. Z. and H-C. C were supported by a NASA grant NAG3-2701 and an NSF grant. M. K. thanks the University of Notre Dame, the ACS Petroleum Research Fund, the NSF

CAREER Program, the Notre Dame Radiation Laboratory and the DOE Office of Basic Energy Sciences for financial support. D. J. thanks C. Wood and Linda Chrisey from the Office of Naval Research for valuable discussions. M. K. and D. J. also thank the Notre Dame Faculty Research Program and the Notre Dame Office of Research for financial support.

### ***Supporting information***

Additional movies illustrating the real time alignment of NWs from solution. Additional movies illustrating the polarization anisotropy of aligned NWs.

### ***References***

1. Patolsky, F.; Lieber, C. M., *Materials Today*, **2005**, 20.
2. Yu, H.; Li, J.; Loomis, R. A.; Gibbons, P. C.; Wang, L.-W.; Buhro, W. E. *J. Am. Chem. Soc.*; **2003**, 125(52); 16168-16169.
3. Grebinski, J. W. ; Richter, K. L. ; Zhang, J.; Kosel, T. H. ; Kuno, M. *J. Phys. Chem. B*, **2004**, 108, 9745; Grebinski, J. W.; Hull, K. L.; Zhang, J.; Kosel, T. H.; Kuno, M. *Chem. Mat.* **2004**, 16, 5260.
4. Peng, Z. A.; Peng, X. G. *J. Am. Chem. Soc.* **2002**, 124, 3343.
5. Mohammad A. I.; Herman, I. P. *Appl. Phys. Lett.*, **2002**, 80(20), 3823-3825.
6. Wu, Y.; Yan, H.; Huang, M.; Messer, B.; Song, J. H.; Yang, P. *Chem. Eur. J.* **2002**, 8, 1261.
7. Khandelwal, A.; Jena, D.; Grebinski, J. W.; Hull, K. L.; Kuno, M. *J. Elec. Mat.*, **2006**, 35, 170.
8. Singh, A. K.; Li, X.; Khandelwal, A.; Kuno M.; Xing, H.; Jena, D. (in preparation)
9. Protasenko V.; Kuno, M. *Adv. Mat.*, **2005**, 17, 2942.

10. Gudiksen, M. S.; Wang, J.; Lieber, C. M. *J. Phys. Chem. B.*, **2001**, 105(19), 4062-4064.
11. Krupke, R.; Hennrich, F.; Lohneysen, H. V.; Kappes, M. M. *Science*, **2003**, 301, 344-347.
12. Alivisatos, A. P. *J. Phys. Chem.* **1996**, 100, 13226; Hu, J. T.; Li, L. S.; Yang, W. D.; Manna, L.; Wang, L. W.; Alivisatos, A. P., *Science*, **2001**, 292, 2060-2063.
13. Shabaev, A.; Efros, Al. L. *Nano Lett.*, **2004**, 4(10), 1821-1825.
14. Robel, I.; Bunker, B.; Kamat, P.; Kuno, M. (submitted)
15. Muljarov, E. A.; Zhukov, E. A.; Dneprovskii, V. S.; Masumoto, Y. *Phys. Review B.*, **2000**, 62(11), 7420-7432.
16. Li, L-S.; Alivisatos, A. P. *Phys. Rev. Lett.* **2003**, 90, 097402-1.
17. Nann, T.; Schneider, J. *Chem. Phys. Lett.* **2004**, 384, 150.
18. Schmidt, M. E.; Blanton, S. A.; Hines, M. A.; Guyot-Sionnest, P. *J. Chem. Phys.* **1997**, 106, 5254.
19. Bernardini, F.; Fiorentini, V.; Vanderbilt, D. *Phys. Rev. B* **1997**, 56, R10024.
20. Smith, P. A.; Nordquist, C. D.; Jackson, T. N.; Mayer, T. S.; Martin, B. J.; Mbindyo, J.; Mallouk, T. E. *Appl. Phys. Lett.* **2000**, 77, 1399.
21. Whang, D.; Jin, S.; Lieber, C. M. *Nano Lett.*, **2003**, 3, 951-954; Whang, D.; Jin, S.; Lieber, C. M. *J. Appl. Phys.* **2004**, 43, 4465.
22. Tao, A.; Kim, F.; Hess, C.; Goldberger, J.; He, R.; Sun, Y.; Xia, Y.; Yang, P. *Nano Lett.* **2003**, 3, 1229.
23. Acharya, S.; Panda, A. B.; Belman, N.; Efrima, S.; Golan, Y. *Adv. Mater.* **2006**, 18, 210.

24. Zhou, R.; Wang, P.; Chang, H.-C. *Electrophoresis*, **2006**, in press.
25. Huang, Y.; Duan, X.; Wei, Q.; Lieber, C. M. *Science*, **2001**, 291, 630.
26. Rothenberg, E.; Kazes, M.; Shaviv, E.; Banin, U., *Nano Lett.*, **2005**; 5(8); 1581-1586.
27. Hull, K. L.; Grebinski, J. W.; Kosel, T. H.; Kuno, M., *Chem. Mat.*, **2005**, 17, 4416.
28. Pohl, H. A. *Dielectrophoresis*. Cambridge University Press, **1978**.
29. Boote, J. J.; Evans, S. D. *Nanotechnology*, **2005**, 16, 1500-1505.
30. Wu, J.; Ben, Y.; Battigelli, D; Chang, H.-C., *Ind. Eng. Chem. Res.*, **2005**, 44 , 2815.
31. *Semiconductors: Other than Group IV Elements and III-V Compounds*. Ed. O. Madelung, Springer Verlag 1992, pg. 29.
32. Shim, M.; Guyot-Sionnest, M. *J. Chem. Phys.* **1999**, 111, 6955.
33. Krishnan, R.; Hahn, M. A.; Yu, Z.; Silcox, J.; Fauchet, P. M.; Krauss, T. D. *Phys. Rev. Lett.* **2004**, 92, 216803-1.
34. Kamat, P. V.; Thomas, K. G.; Barazzouk, S.; Girishkumar, G.; et al. *J. Am. Chem. Soc.*, **2004**, 126, 10757-10762.
35. Chen, X. Q.; Saito, T. *Appl. Phys. Lett.*, **2001**, 78(23) 3714-3716.
36. Kagan, C. R.; Murray, C. B.; Bawendi, M. G. *Phys. Rev. B* **1996**, 54, 8633.
37. Empedocles, S. A.; Bawendi, M. G. *Science* **1997**, 278, 2114.
38. Patolsky, F.; Zheng, G.; Hayden, O.; Lakadamyali, M.; Zhuang, X.; Lieber, C. M. *Proc. Natl. Acad. Sci.* **2004**, 101, 14017.